IEEE Access
Multidisciplinary ⋮ Rapid Review ⋮ Open Access Journal

Received May 14, 2021, accepted June 1, 2021, date of publication June 18, 2021, date of current version June 30, 2021.

Digital Object Identifier 10.1109/ACCESS.2021.3090657

An Average Consensus Algorithm for Seamless Synchronization of Andronov-Hopf Oscillator Based Multi-Bus Microgrids

IGOR SOWA[1], TRUNG THAI TRAN[1,2], TOBIAS HEINS[1], DAVID RAISZ[1,3], (Senior Member, IEEE), AND ANTONELLO MONTI[1], (Senior Member, IEEE)

[1]Institute for Automation of Complex Power Systems, RWTH Aachen University, 52074 Aachen, Germany
[2]Faculty of International Training, Thai Nguyen University of Technology, Thai Nguyen 24000, Vietnam
[3]Department of Electrical Power Engineering, Budapest University of Technology and Economics, 1111 Budapest, Hungary

Corresponding author: Igor Sowa (isowa@eonerc.rwth-aachen.de)

This work was supported by the German Federal Ministry for Education and Research through the Project Kopernikus Ensure Phase 2 under Grant 03SFK1C0-2.

ABSTRACT This study proposes a hierarchical control structure for a smooth transition of multi-bus microgrids from islanded mode to grid-connected mode. The proposed control structure uses an average consensus protocol for the secondary control layer and Andronov-Hopf virtual oscillator control as a primary controller. The proposed method enhances the power-sharing accuracy among DGs in normal operation. A synchronization strategy is embedded into the secondary control layer in synchronization mode to force the MG-side voltage at the connection point to synchronize with the grid-side voltage. The influence of the secondary controller and communication time-delay on system stability and performance is analyzed with small-signal analysis. The proposed method is validated via control-hardware-in-the-loop (CHiL) using a real-time Opal-RT platform.

INDEX TERMS Distributed generation, microgrids, power-sharing control, synchronization, power system dynamics, power system stability.

I. INTRODUCTION

The growth of economic and environmental concerns is pushing the conventional centralized power systems to evolve toward a distributed, local paradigm with innovative business models. This trend aims at integrating more distributed generation (DG) close to the consumers' area, thus increasing the system reliability, quality and reduce the cost. DGs and the local consumers in the same geographic location form a small-scale power system named a Microgrid (MG) [1]. The most important feature of MGs is the capability to operate in both autonomous (islanded) and grid-connected modes. In islanded mode, MGs lose the stable voltage and frequency support from the utility grid and needs to balance the load demand and power generation by themselves. This load/generation balancing results in the *voltage asynchronism* that may cause severe problems at the moment of reconnection to the main grid [2], such as power oscillations or significant inrush current flowing through the static switch. Therefore, to ensure an uninterruptable and reliable power supply, as well as to maintain system stability, a smooth transient is required, i.e. the MG voltage must be synchronized with the main grid voltage before reconnection.

Generally, power-electronic-based interfaces of DGs (also known as Voltage Source Converter - VSC) in a MG are controlled by a hierarchical control structure. An example of a droop-based hierarchical control structure is depicted in Fig. 1a, in which the synchronization mechanism is embedded in the secondary control layer. The main drawbacks of this control structure are the complexity of multiple control layers and the slow dynamic response due to the time-scale separation between control layers. To overcome the limitations of conventional droop-based control structure, several improved methods have been proposed, such as in [3], [4]. In [3], an improved droop control based on the virtual power source and composite virtual impedance is presented

The associate editor coordinating the review of this manuscript and approving it for publication was Tariq Masood.

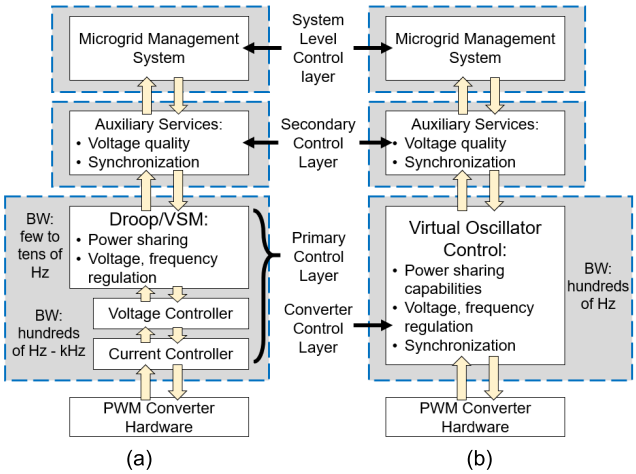

FIGURE 1. Typical hierarchical control structure in VSC-based MGs: a) droop/VSM based MGs, b) VOC-based MGs.

to enhance the accurate reactive power sharing and reduce the coupling of DG power outputs. In [4], the authors proposed two additional correction terms of voltage reference to simultaneously provide economic load sharing and global bus voltage regulation. Recently, virtual oscillator control (VOC) has been introduced and expected to provide better overall performance than the conventional droop control method [5]. A possible control hierarchy of VOC-based MGs is shown in Fig. 1b, in which the functions of the converter control layer also involve the power-sharing capability and voltage, frequency regulation. As VOC technology shows promising advantages over droop control, this work focuses on its application in multi-bus MGs and designing a suitable synchronization solution to seamlessly synchronize a multi-bus MG to the main grid.

Various synchronization techniques have been proposed in the literature, which can be categorized in different ways. In this work, we analyze two groups of synchronization solutions considering MG topology as follows: i) synchronization of an individual DG to an energized grid, or MG with a single DG, or a master DG in MG using master-slave control strategy [5]–[8], and ii) synchronization of MGs with several DGs and complex topologies, i.e., multi-bus MGs. The solutions for the first group are relatively simple, in comparison with the second group since the synchronization control signal only needs to send from the synchronization controller to a single (master) DG. In [5], a simple synchronization control method is embedded into the VOC system to connect/disconnect a single VOC-based DG to/from an energized microgrid, by enforcing DG output voltage to be equal to the grid-side voltage at the connection point. However, this method is not suitable for synchronizing an MG with several VOC-based DGs to the main utility grid since it requires a centralized communication network to send time-domain voltage signals to every single DG. Also, in the multi-bus MG application with local loads connected near DG locations, enforcing all DG output voltages to be equal to grid-side PCC voltage may significantly influence the power flow on the network. A universal integrated synchronization and control method that is analogous to the virtual synchronous machine technique is proposed in [6] to synchronize a single DG to the main grid. However, the power reference signals need to be set equal to zero during the transition process, making it not applicable for synchronizing an energized multi-bus MG to the main grid. In [7], a frequency-locked-loop (FLL)-based synchronization method is used in MG with master-slaver configuration. However, the change of control mode may cause large transient oscillations in a short period. The PLL-based synchronization method is presented in [8] to generate synchronization reference signals (frequency and voltage) for the master inverter. However, this method still has issues related to the PLL technique, e.g., nonlinearity characteristics, inherently noise sensitive, expensive, and difficulty in implementation.

The synchronization solutions for group ii) are more challenging than for group i) because a multi-bus MG comprises multiple DGs with distinct characteristics and a lot more communication links between them (in the case of hierarchical control structure). Improper design of synchronization algorithms may result in failure to synchronize, causing severe system oscillations and even destabilizing the whole system. In practice, the MG synchronization is controlled by a signal from the *synchroscope* with *synchcheck* relay, which closes the static switch when the synchronization requirements are fulfilled. However, this method usually involves human activities that cause inconsistent results. An active synchronization method using MG central controller is proposed in [9] for a multi-bus MG. However, the centralized method is vulnerable to single-point failure and can increase investment costs when the number of DGs increases. In [2], a distributed synchronization framework is proposed for reconnecting a multi-bus MG to the utility grid. The synchronization signals are sent to several DGs (usually called leading DGs), and the consensus-based distributed protocol regulates the frequency and voltage of all DGs to enforce the voltage at the MG-side of the static switch (SS) to slowly synchronize with the one at the main grid side. The distributed active synchronization strategy in [10] takes into account both fundamental and negative and zero sequence components of the voltage so that the transient of the synchronization method is not affected by distorted loads.

This paper presents the design of an autonomous synchronization method for the multi-bus MG controlled with VOC, which is based on an average consensus distributed protocol (CDP). With the proposed method, all DGs adjust their active, reactive power output in a cooperative manner to regulate the voltage of MG to track the main grid voltage. The main contributions of this paper are as follows: i) an average consensus distributed protocol that uses only a spare communication network is proposed to achieve the load power-sharing among DGs and autonomous synchronization simultaneously; thus, the problem related to single-point failure no longer exists, ii) An improvement of the

Andronov-Hopf Oscillator (AHO) [11] is presented to control DGs in both islanded and grid-connected multi-bus MG, and iii) the proposed synchronization framework does not require direct frequency and phase angle measurement to track magnitude, frequency, and phase angle of the grid voltage. It should be noted that there are different distributed methods that might be suitable for the mentioned synchronization issue, such as delay-tolerant power compensation control [12], and event-triggered method [13]. However, the goal of this study is not to compare all the available methods, but to find a simplest and most reliable method for ensuring proper synchronization of AHO-based MGs to the main grid. Therefore, the CDP is chosen.

The remainder of this paper is organized as follows: in section II, a hierarchical control structure of a multi-bus MG with the detailed modification of AHO is presented. Section III briefly presents standard requirements and the basis of synchronization process. The proposed distributed synchronization framework is developed in section IV. Section V validates the performance of the proposed method. Section VI concludes the paper.

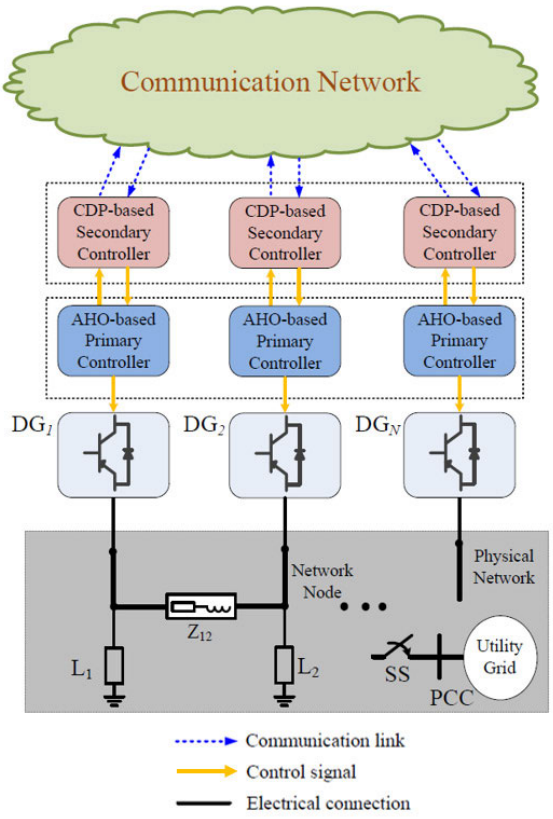

FIGURE 2. Multi-bus Microgrid with hierarchical control structure.

II. HIERARCHICAL CONTROL STRUCTURE OF A MULTI-BUS MICROGRID

The structure of a multi-bus MG with N DG units is presented in Fig. 2. DG units connect to each other and to the main utility grid through a physical network. The loads can be connected locally near the DG area or at a common bus between two DG units. The hierarchical control structure of each DG adopted in this work consists of two main layers, i.e., the primary and secondary control. The primary control layer uses improved AHO to stabilize the local voltage and frequency, and provides a desired power-sharing mechanism.

The average consensus distributed protocol is adopted as secondary control layer to implement: i) a correction mechanism to nullify the power-sharing inaccuracy caused by impedance mismatches, nonidentical feeder impedance and parameter drifts, ii) an autonomous synchronization strategy under the request from higher control level which is not a scope of this work. The proposed hierarchical control structure uses only low bandwidth, spare communication network to exchange information between a DG and its neighbors (in case of autonomous MG operation) and between leading DGs and synchronization controller SC (during the synchronization process). The neighboring relation of each DG can be defined either by electrical topology or other topologies considering economic aspect and must fulfill requirements of the graph theory (see Section 4.2 for the detail).

III. BASIS OF SYNCHRONIZATION IN MULTI-BUS MG

Fig. 3 presents a single-line diagram of the tested multi-bus MG in which the utility grid is connected to the MG via the SS. The utility grid is assumed to be the swing bus, which imposes fixed nominal voltage and frequency, and the DGs are operated in the grid-supporting mode. The blue dashed line represents the communication between DGs and the utility grid. The status of SS defines the operating mode of MG, i.e., when SS closes, MG is connected to the utility grid, and vice versa. In islanded mode, the loads cause the MG voltage (magnitude and frequency) to deviate from the nominal values and consequently influence the mismatch Δv between voltages at two sides of the SS, i.e., the voltage at bus A and B in Fig. 2. The error term Δv contains information of both voltage magnitude, frequency and phase angle deviation.

The value of Δv at the moment of reconnection defines the consequent level of the asynchronism, ranging from small power oscillations, overvoltage, significant inrush current to system instability, and equipment damage. To prevent the adverse impacts of the asynchronism on system stability and quality, it is required to keep the value of Δv within a strict limit for a specific time period before reconnecting the MG to the utility grid. As the tested MG has the average DG rating from 0 to 500 kVA, the synchronization requirement according to the IEEE Standard 1547.2-2008 are as follow: the maximum allowed tolerances of the voltage magnitude and phase angle are $\pm 10\%$, $\pm$ 20 degree, respectively; and the frequency tolerance is 0.3 Hz.

The basic concept of autonomous synchronization is to force the voltage deviation Δv to stay within the standard limit before closing the SS. The information of Δv is pre-processed by using a simple calculation (see Section 4.2) and sent to the CDP of one or several leading DGs while the

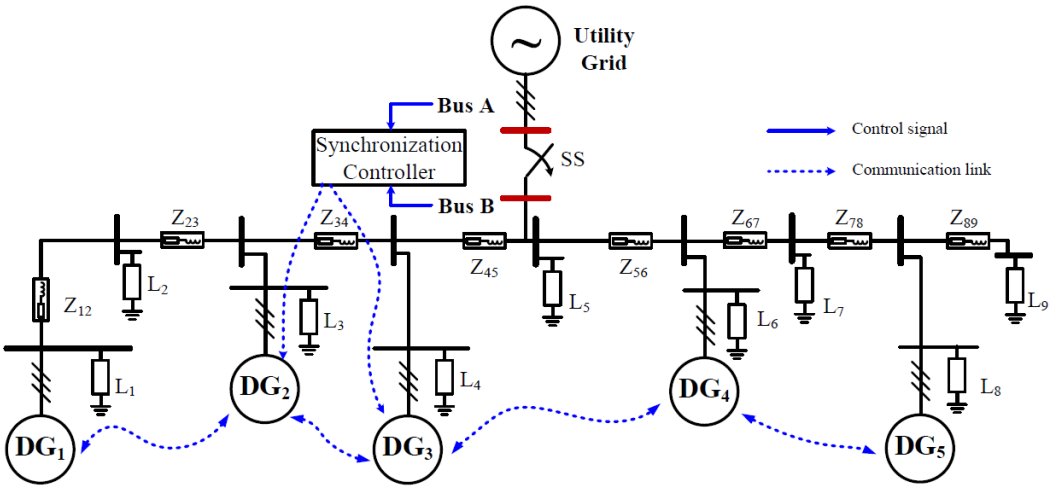

FIGURE 3. A multi-bus MG connected to the utility grid via a static switch.

rest of DGs remain information exchange with its neighbors. The detail of these control signals and corresponding modifications of the CDP control laws are presented in the next sections.

IV. PROPOSED DISTRIBUTED HIERARCHICAL CONTROL FRAMEWORK

In this section, the proposed control framework is presented in detail. First, the basis of AHO with its potential technical challenges in the multi-bus MG scenario is discussed. The necessary modification is presented to improve controller performance and the possibility of adopting AHO into multi-bus MGs. Then, the synchronization control strategy based on average consensus distributed protocol is proposed to actively synchronize the MG voltage with the main utility grid before closing the static switch.

A. ANDRONOV-HOPF OSCILLATOR CONTROL

AHO is an advanced VOC strategy that has been developed and is expected to solve the shortcomings of previous VOC methods in the literature [14]. In comparison, the main advantages of AHO are: i) the elimination of third-order harmonics in the oscillators voltage signal and thus the removal of a design trade-off between transient performance and voltage quality, ii) the embedment of setpoints for power dispatching makes AHO suitable for both grid-connected and islanded operation. Fig. 4 shows the general structure of AHO applied to a three-phase VSC-based DG. Unlike Van der Pol type VOC, AHO uses both alpha and beta components of the orthogonal errors between the filter inductor current $i_{\alpha,\beta}$ and current reference $i^*_{\alpha,\beta}$, i.e., $\Delta i = i_{\alpha,\beta} - i^*_{\alpha,\beta}$, so that it is applicable for three-phase application even under unbalanced conditions. The rotating matrix $\begin{bmatrix} cos(\vartheta) & -sin(\vartheta) \\ sin(\vartheta) & cos(\vartheta) \end{bmatrix}$ plays a key role in defining the droop relation between AHO output

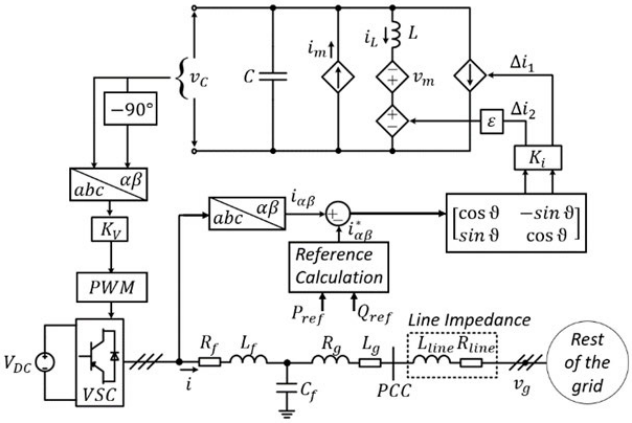

FIGURE 4. Schematic diagram of three-phase VSC-based DG with AHO.

voltage and frequency and active, reactive power generation. The value of ϑ is chosen based on the grid impedance angle.

The dynamic of AHO can be briefly explained as follows. To achieve the desired oscillator dynamic of the capacitor voltage, a nonlinear state-dependent voltage, and current source v_m and i_m are used in the AHO circuit to force the oscillation to its asymptotic trajectory by absorbing and injecting energy. Applying Kirchhoff's current and voltage law to the AHO circuit in Fig. 4, the equations that govern the dynamics of AHO are formulated as follows:

$$C\frac{dv_C}{dt} = -i_L + i_m - \Delta i_1 \tag{1}$$

$$L\frac{di_L}{dt} = v_C + v_m - \varepsilon\Delta i_2 \tag{2}$$

Here, $v_m = \frac{\xi}{\omega_n}\left(2X_n^2 - \|x\|^2\right)\varepsilon i_L$ and $i_m = \frac{\xi}{\varepsilon\omega_n}\left(2X_n^2 - \|x\|^2\right)v_C$, where X_n defines the amplitude of the oscillators limit cycle, ω_n is the nominal system frequency and ξ governs the speed of convergence to steady-state.

$\|x\|$ is the Euclidean norm of vector $x = \left[\, v_C \;\; \varepsilon i_L \,\right]^T, x \in \mathbb{R}^N$. From (1) and (2), and the elemental definitions of voltage magnitude, angle, active and reactive power in $\alpha\beta$ coordinate, the dynamic model of AHO in terms of voltage magnitude V_C and phase angle θ is derived as follows:

$$\dot{V}_C = \frac{\xi}{K_v^2} V_C \left(2V_n^2 - 2V_C^2\right) - \frac{K_v K_i}{3CV_C} \left(sin\left(\vartheta\right)\left(Q - Q_{ref}\right) + cos\left(\vartheta\right)\left(P - P_{ref}\right)\right) \tag{3}$$

$$\dot{\theta} = \omega_n - \frac{K_v K_i}{3CV_C^2} \left(sin\left(\vartheta\right)\left(P - P_{ref}\right) - cos\left(\vartheta\right)\left(Q - Q_{ref}\right)\right) \tag{4}$$

where V_n is the nominal RMS voltage magnitude, K_v and K_i are voltage and current scaling factors to couple AHO input and output to physical electrical feedback signals, respectively. The active, reactive power setpoints P_{ref} and Q_{ref} from system control level are used to calculate the current reference signals. The detailed derivation of (3) and (4), as well as the design specifications, can be found in [14].

In literature, AHO only prioritizes the power dispatch in grid-connected operation based on commands from upper control level. On the contrary, the islanded operation, especially the power-sharing among DGs and seamless synchronization for reconnection with the main grid, has not been mentioned. With our proposed algorithm, we are addressing both applications.

In this section, we conduct a comprehensive discussion on the islanded operation of a multi-bus MG with AHO-based DGs. In islanded mode, the power reference signals of all DGs are set equal to 0, i.e., $P_{ref} = Q_{ref} = 0$. By doing this, the dependency of AHO on reference signals from the control center is neglected. The load power is shared among DGs in proportion to VSC-rated powers, achieved by appropriately setting AHO parameters. By setting the derivatives $\dot{v_C} = 0$ and $\dot{\theta} = \omega$, the equilibria of voltage and frequency of VSC in islanded mode are defined as follows:

$$V_C = \frac{V_n}{\sqrt{2}} \left(1 + \sqrt{1 - \frac{2K_i K_v^3}{3C\xi V_n^4} \left(sin\left(\vartheta\right) Q + cos\left(\vartheta\right) P\right)}\right)^{1/2} \tag{5}$$

$$\omega = \omega_n - \frac{K_v K_i}{3CV_C^2} \left(sin\left(\vartheta\right) P + cos\left(\vartheta\right) Q\right) \tag{6}$$

Equations (5) and (6) show the relation between AHO output voltage magnitude and frequency corresponding to a specified active, reactive power output. The accuracy of the load power-sharing is dependent on the ratio of equivalent impedances seen from the DGs, and requires that it is proportional to the desired power-sharing ratio. In an LV multi-bus MG, the equivalent impedance is challenging to obtain, or even unknown because of its complex topology and the diverse position of the loads. Hence, the power-sharing inaccuracy is inevitable and needs to be compensated. Also, (5) and (6) indicate the deviation from the nominal values of V_C and ω proportional to the active and reactive power output, causing the MG to lose synchronism with the main grid. Consequently, it is required to have an SC to guarantee a fast and seamless transition between islanded and grid-connected modes. In this paper, the control strategy is integrated into the AHO circuit to adaptively regulate the internal parameters of AHO (V_n and ω_n) based on desired control requirements. Therefore, the following modifications of (5) and (6) are made:

$$V_C = \frac{V_n + \Delta V_n}{\sqrt{2}} \left(1 + \sqrt{1 - \frac{2}{C\xi * S_r} \left(sin(\vartheta) Q + cos(\vartheta)\, P\right)}\right)^{1/2} \tag{7}$$

$$\omega = \left(\omega_n + \Delta\omega_n\right) - \frac{\left(V_n + \Delta V_n\right)^2}{CV_C^2 * S_r} \left(sin\left(\vartheta\right) P - cos\left(\vartheta\right) Q\right) \tag{8}$$

Here, ΔV_n and $\Delta\omega_n$ are determined by the following adaptive control law to regulate AHO power output:

$$\frac{d}{dt}\Delta V_n = K_{\Delta V} \left(sin\left(\vartheta\right)\left(Q - Q_{ave}\right) + cos\left(\vartheta\right)\left(P - P_{ave}\right)\right) \tag{9}$$

$$\frac{d}{dt}\Delta\omega_n = K_{\Delta\omega} \left(sin\left(\vartheta\right)\left(P - P_{ave}\right) - cos\left(\vartheta\right)\left(Q - Q_{ave}\right)\right) \tag{10}$$

where $K_{\Delta V}$ and $K_{\Delta\omega}$ are the control gains that determine the convergence speed of the proposed method. The control laws in (9) and (10) regulate the magnitude and phase angle of AHO voltage output and consequently force the power output of the DGs to follow the setpoints P_{ave} and Q_{ave} which are defined by the proposed CDP. The functions of the power setpoints are: i) to guarantee accurate power-sharing among DGs in normal islanded operation, and ii) synchronization with the main grid for a seamless transition from islanded to grid-connected operation. The details of the CDP are presented in the subsequent section.

B. PROPOSED DISTRIBUTED FRAMEWORK FOR POWER-SHARING CONTROL AND SYNCHRONIZATION

An illustration of the proposed controller is shown in Fig. 5. Each DG, as presented in Fig. 5, has access only to its local measurement. The proposed CDP of $\mathrm{DG_i}$ receives information of the neighboring power output (P_j, Q_j) through the communication network. The filtered power output of DGs, P_j and Q_j, is calculated by using instantaneous power concept in alpha/beta coordinates. The proposed control strategy has two main functions, based on the operation mode of the MG. In normal islanded operation, CDP detects power-sharing errors among DGs, and reaches a global consensus average value by iteratively exchanging and updating the power setpoints. In synchronization mode, the voltage magnitude and phase angle error between the grid (bus A) and MG sides (bus B) of the static switch are sent to the CDP of one or several leading DG(s) while the rest of the DGs remain information exchange with only its neighbors. The additional synchronization control signals δ_v, δ_ω and δ_θ force the CDP

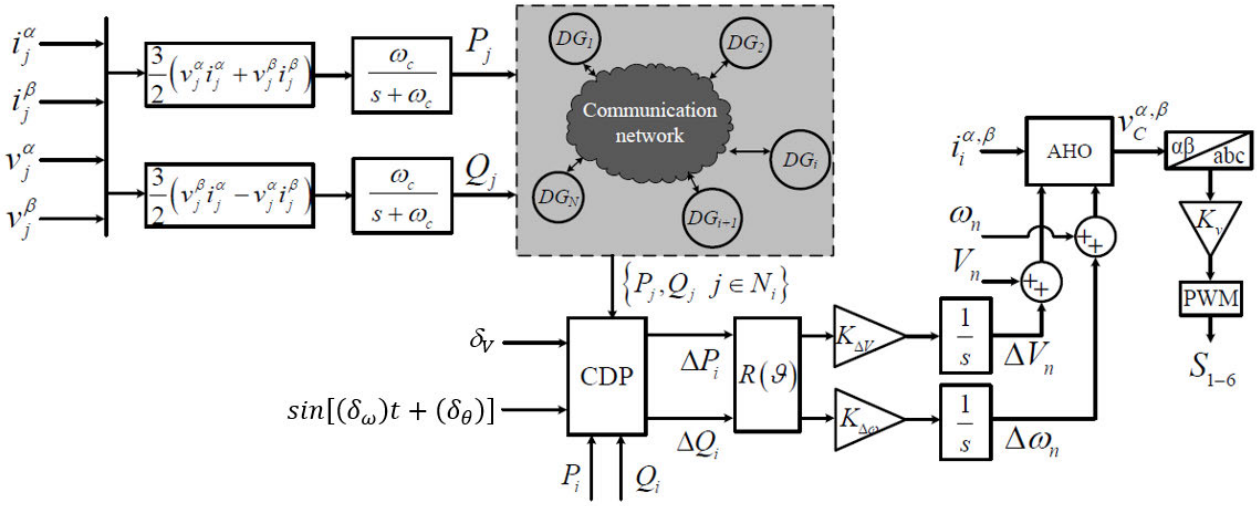

FIGURE 5. The diagram of a DG in the proposed distributed framework.

of the leading DG(s) to find a new consensus value in which Δv is within standard synchronization limits. The remaining DGs follow the change of the leading DG(s) through the CDP by updating their power setpoints in dependency of the neighboring power output. At the new steady state in which the voltage at points A and B are synchronized, the MG can seamlessly connect to the main grid without a significant transient.

The average consensus distributed control algorithm is based on graph theory. The following paragraph introduces the basics of Graph Theory and its application in the distributed average consensus control for multi-bus MG.

Considering a directed graph G with N nodes and m edges, an adjacency matrix $\boldsymbol{A} = [a_{ij}] \in \mathbb{R}^{N\times N}$ showing the connection between node i and node j, in which $a_{ij} = 1$ if there is a communication link and $a_{ij} = 0$ otherwise. The graph G has a spanning tree as a sub-graph of G if the corresponding Laplacian matrix $\boldsymbol{L}$ of G is defined as $\boldsymbol{L} = \boldsymbol{D} - \boldsymbol{A}$, where $\boldsymbol{D} = diag\left(\sum_{j\in N_i} a_{ij}\right) \in R^{N\times N})$ is the in-degree matrix and $N_i = \{j \in N : (i,j) \in m\}$ is the neighbors of node i. A spanning tree is required in order to guarantee at least one communication link to each node. Based on information exchange between each node and its neighbors, a distributed average consensus control forces the state of all nodes in the network to reach a common equilibrium point. Assuming $x(0) = [x_1(0), x_2(0), \ldots, x_N(0)]^T$ is the initial condition of each node in the network, as long as there exists a spanning tree of the graph G, after a finite step K, the value of all nodes converges to an average value defined as follows:

$$x(K) = \frac{1}{N}\sum x_i(0) \tag{11}$$

Applying graph theory to a multi-bus MG, the communication network is considered as an undirected graph in which each DG is represented as a node, and a communication link between DG_i and DG_j is an edge. A discrete-time representation of CDP for a DG_i is as follows:

$$x_i^{(k+1)} = x_i^{(k)} + G_i \sum_{j\in N_i} \mu_{ij}\left[K_i x_i^{(k)} - K_j x_j^{(k)}\right] \tag{12}$$

where, $x_i^{(k)} = \left[P_i^{(k)} Q_i^{(k)}\right]^T$ and $x_j^{(k)} = \left[P_j^{(k)} Q_j^{(k)}\right]^T$ is the local information of the states (active and reactive power) of DG_i and DG_j at the step k, respectively. The gain $K_i = \left[K_{iP} K_{iQ}\right]^T$ and $K_j = \left[K_{jP} K_{jQ}\right]^T$ is chosen according to the power sharing ratio $\frac{P_i}{K_{iP}} = \frac{P_j}{K_{jP}}$, and $\frac{Q_i}{K_{iQ}} = \frac{Q_j}{K_{jQ}}$. If there is a communication link between DG_i and DG_j, the factor $\mu_{ij} = 1$, while $\mu_{ij} = 0$ otherwise. The weighted factor G_i plays a significant role in guaranteeing system stability during the information exchange and increase the convergent speed.

When the communication network of a multi-bus MG has a spanning tree, the proposed CDP drives the states of DGs toward an average consensus value after a finite step K, as follows:

$$\begin{bmatrix} P_{ave}^{(K)} & Q_{ave}^{(K)} \end{bmatrix}^T = \begin{bmatrix} \frac{1}{K_{iP}} \frac{\sum_{i=1}^{N} K_{iP} P_i^{(0)}}{N} & \frac{1}{K_{iQ}} \frac{\sum_{i=1}^{N} K_{iQ} Q_i^{(0)}}{N} \end{bmatrix}^T \tag{13}$$

Applying (13) into control law in (9) (10), the value of V_n and ω_n is adaptively adjusted and the power outputs of all DGs in MG reach the average consensus value.

In synchronization mode, the voltage at bus A and B are centrally measured and sent to the SC located at the static switch for data pre-processing. Then, the control signals from the SC are sent to the CDP of one or several leading DG(s) while the rest of the DGs remain information exchange with its neighbors. The magnitude δ_V, angular frequency δ_ω and phase angle δ_θ of this voltage error are achieved by the

following equation:

$$\delta_V = |V_A| - |V_B| \tag{14}$$
$$\delta_\omega = \omega_A - \omega_B \tag{15}$$
$$\delta_\theta = \theta_A - \theta_B \tag{16}$$

The magnitude difference can be calculated easily by using (14). However, due to the periodic feature of the off-nominal sine wave, the measured phase angle varies between $[-\pi, \pi]$ with the abrupt changes at the value of $-\pi$ and π. Therefore, directly using the measured phase angle as an input for a controller may result in unexpected oscillations and longer settling time. Instead, in this paper, an alternative approach is proposed as follows.

Let the three-phase voltages at bus A be $v_{A\_a} = \sqrt{2}\,|V_A|\,cos\,(\omega_A t + \theta_A)$, $v_{A\_b} = \sqrt{2}\,|V_A|\,cos\left(\omega_A t + \theta_A - \frac{2\pi}{3}\right)$, and $v_{A\_c} = \sqrt{2}\,|V_A|\,cos\left(\omega_A t + \theta_A + \frac{2\pi}{3}\right)$, respectively. Similarly, the three-phase voltages at bus B are $v_{B\_a} = \sqrt{2}\,|V_B|\,cos\,(\omega_B t + \theta_B)$, $v_{B\_b} = \sqrt{2}\,|V_B|\,cos\left(\omega_B t + \theta_B - \frac{2\pi}{3}\right)$, and $v_{B\_c} = \sqrt{2}\,|V_B|\,cos\left(\omega_B t + \theta_B + \frac{2\pi}{3}\right)$. Using Clarke Transformation yields:

$$\begin{aligned} V_{A,\alpha} &= |V_A|\,cos\,(\omega_A t + \theta_A) \\ V_{A,\beta} &= |V_A|\,sin\,(\omega_A t + \theta_A) \end{aligned} \tag{17}$$

and

$$\begin{aligned} V_{B,\alpha} &= |V_B|\,cos\,(\omega_B t + \theta_B) \\ V_{B,\beta} &= |V_B|\,sin\,(\omega_B t + \theta_B) \end{aligned} \tag{18}$$

By using (17) and (18), the following expression can be derived:

$$\begin{aligned} &V_{A,\beta}V_{B,\alpha} - V_{B,\beta}V_{A,\alpha} \\ &\quad = |V_A|\,|V_B|\,sin\,(\omega_A t + \theta_A)\,cos\,(\omega_B t + \theta_B) \\ &\qquad - |V_A|\,|V_B|\,sin\,(\omega_B t + \theta_B)\,cos\,(\omega_A t + \theta_A) \\ &\quad = |V_A|\,|V_B|\,sin\,[(\omega_A - \omega_B)\,t + (\theta_A - \theta_B)] \end{aligned} \tag{19}$$

Dividing two side of (19) for $|V_A|\,|V_B|$ yields:

$$\delta_{syn} = \frac{V_{A,\beta}V_{B,\alpha} - V_{B,\beta}V_{A,\alpha}}{|V_A|\,|V_B|} = sin\,[(\delta_\omega)\,t + (\delta_\theta)] \tag{20}$$

It can be seen from (20) that the right term $sin\,[(\delta_\omega)\,t + (\delta_\theta)]$ contains information of not only the phase angle difference but also the frequency mismatch between the voltage at bus A and bus B. It is obvious that $sin\,[(\delta_\omega)\,t + (\delta_\theta)] = 0$ if both δ_ω and δ_θ equal to zero. Therefore, the term $sin\,[(\delta_\omega)\,t + (\delta_\theta)]$ can be used as a control variable for frequency and phase angle tracking.

In the proposed active synchronization control strategy, to force the bus B voltage to track that of bus A, the magnitude tolerance δ_V is added into the active power control law of CDP of one or several leading DG(s). Meanwhile the angular frequency tolerance δ_{syn} is added to reactive power control law as follows:

$$\begin{aligned} \frac{d}{dt}\delta_{V_n} = K_{\Delta V}\,&\left(sin\,(\vartheta)\,\left(Q - Q_{ave} - \gamma_{syn}K_{|\omega-\theta|}\delta_{syn}\right)\right. \\ &\left. + cos\,(\vartheta)\,\left(P - P_{ave} - \gamma_{syn}K_{|\Delta V|}\delta_V\right)\right) \end{aligned} \tag{21}$$

$$\begin{aligned} \frac{d}{dt}\delta_{\omega_n} = K_{\Delta\omega}\,&\left(sin\,(\vartheta)\,\left(P - P_{ave} - \gamma_{syn}K_{|\Delta V|}\delta_V\right)\right. \\ &\left. - cos\,(\vartheta)\,\left(Q - Q_{ave} - \gamma_{syn}K_{|\omega-\theta|}\delta_{syn}\right)\right) \end{aligned} \tag{22}$$

Here, $K_{|\Delta V|}$ and $K_{|\omega-\theta|}$ are the corresponding coefficients for voltage magnitude and angular frequency tracking, respectively. The synchronization control is activated if $\gamma_{syn} = 1$, and is deactivated otherwise.

As seen from (21) and (22), when the synchronization mode is activated, the active and reactive power control laws of the proposed CDP now include tracking errors from (14) and (20). The CDP of the leading DG(s) only shift up/down their operating curves according to the received synchronization signals, i.e. $K_{|\Delta V|}\,|\delta_V|$ and $K_{|f-\theta|}sin\,[(\delta_\omega)\,t + (\delta_\theta)]$. The remaining DGs then follows the change of the leading DG(s) in a distributed manner. At the steady-state of the synchronization process, $|\delta_V| = 0$ and $\delta_{syn} = 0$; then, the control law in (21) and (22) becomes the original control of active power sharing control in (9) and (10). Therefore, the power-sharing function of the CDP is not affected.

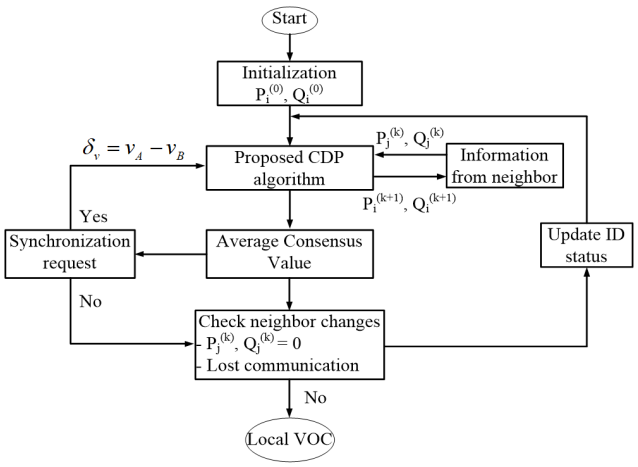

FIGURE 6. Flow chart of the proposed CDP.

A brief flow chart of the proposed algorithm is presented in Fig. 6. The initial values of active and reactive power of DG_i ($P_i(0)$, $Q_i(0)$) and power information from its neighbors are used to calculate the references for power outputs of DG_i in the next iteration. After a finite iteration K, the power outputs of DG_i reach an average consensus value defined by (13). The synchronization request forces the proposed CDP of DG_i to update the algorithm to find a new equilibrium point where the voltages at both sides of the static switch are synchronized. The proposed method continuously observes the status of DGs in MG by checking the status of the communication links and perform necessary modifications, e.g., if the communication between DG_i and DG_j is lost, the CDP of DG_i removes DG_j from the list of neighbors and implements algorithm with a new set of inputs.

C. SMALL-SIGNAL STABILITY ANALYSIS OF SECONDARY CONTROL FOR POWER SHARING

An eigenvalue-based small-signal analysis is performed in this section to analyze the impact on the stability of secondary

controller parameters and communication delay for power-sharing capabilities. The analysis is performed on a multi-bus MG consisting of N VOC-based DGs, M buses connected through B branches (see [15] for the detailed configuration of the model). The model of the considered MG for small-signal stability analysis is achieved through linearization of equations of the components of the system, including VSCs with VOC-based primary control, the electrical topology of the system described through and branches and buses (nodes) with RL loads, as well as the secondary controller with communication links topology. The proposed synchronization algorithm is excluded from this stability analysis as being beyond the scope of the small-signal model, and the synchronous conditions are assumed setting $|\delta_V| = 0$ and $\delta_{syn} = 0$.

The linearization of the proposed secondary controller in (21) and (22) around a specific operating point yields the following:

$$\Delta\dot{\delta}_{V,i} = K_{\Delta V}\left[\sin(\vartheta)\left(\frac{N_i+2}{N_i+1}\Delta q_i - \frac{1}{N_i+1}\sum_{j\in\underline{N}_i}^{N}\Delta q_j\right) + \cos(\vartheta)\left(\frac{N_i+2}{N_i+1}\Delta p_i + \frac{1}{N_i+1}\sum_{j\in\underline{N}_i}^{N}\Delta p_j\right)\right] \forall i\epsilon\underline{N} \tag{23}$$

$$\Delta\dot{\delta}_{\omega,i} = K_{\Delta\omega}\left[\sin(\vartheta)\left(\frac{N_i+2}{N_i+1}\Delta p_i - \frac{1}{N_i+1}\sum_{j\in\underline{N}_i}^{N}\Delta p_j\right) - \cos(\vartheta)\left(\frac{N_i+2}{N_i+1}\Delta q_i + \frac{1}{N_i+1}\sum_{j\in\underline{N}_i}^{N}\Delta q_j\right)\right] \forall\, i\epsilon\underline{N} \tag{24}$$

where $\underline{N}_i$ is a set of neighbors of the i-th DG; Δp_i, Δp_j and Δq_i, Δq_j are linearized equations for the active and reactive power of i-th and j-th DG, respectively, which are derived from the equations to define power injection of DG_i to the rest of the grid through an equivalent impedance $Z_{c,i} = R_{c,i} + sL_{c,i}$, as follows:

$$\begin{bmatrix} P_i \\ Q_i \end{bmatrix} = \begin{bmatrix} v^d_{VOC,i} & v^q_{VOC,i} \\ v^q_{VOC,i} & -v^d_{VOC,i} \end{bmatrix}\begin{bmatrix} i^d_{o,i} \\ i^q_{o,i} \end{bmatrix} \quad \forall\, i\epsilon\underline{N} \tag{25}$$

where, $i^d_{o,i}$ and $i^q_{o,i}$ denote the values of the in-phase (d) and quadrature-phase (q) components of the DG output currents $i_{o,i}$. The d- and q-components of the i-th VOC-based DG output voltage are expressed as:

$$\begin{aligned} v^d_{VOC,i} &= v_{VOC,i}cos\left(\theta_{VOC,i}\right) \\ v^q_{VOC,i} &= v_{VOC,i}\sin\left(\theta_{VOC,i}\right) \end{aligned} \tag{26}$$

Using a linearized model of a multi-bus MG exclusively presented in [15], the AHO model in (7) and (8), and the linearized model of the proposed secondary controller in (23) and (24), the complete dynamic model of the tested system which considers communication time delays can be formulated in a compacted form as $\mathbf{\Delta\dot{x}}(t) = \boldsymbol{A_0}\mathbf{\Delta x}(t) + \boldsymbol{A_1}\mathbf{\Delta x}(t-\tau_d)$, where $\mathbf{\Delta\dot{x}}$ is the vector of linearized state variables based on the equations linearized (3)-(4), equations (23)-(24), as well as on linearized output currents of DGs, load currents, and branch currents. The matrices $\boldsymbol{A_0}$ and $\boldsymbol{A_1}$ are the state matrices of the same size corresponding to ordinary and delayed state variables τ_d, respectively. $\boldsymbol{A_0}$ and $\boldsymbol{A_1}$ can be derived by calculating partial derivatives $\frac{\partial\mathbb{F}}{\partial X}$ of the nonlinear system. In order to analyze the stability of the time-delayed system $\mathbf{\Delta\dot{x}}(t)$, its eigenvalues need to be calculated from the roots of the following transcendental characteristic equation:

$$det\left(s\boldsymbol{I_0} - \boldsymbol{A_0} - \boldsymbol{A_1}e^{-s\tau_d}\right) = 0 \tag{27}$$

By using (27) and the parameters shown in Table 1 and 2, the root locus of the dominant eigenvalues of the 5-DG/9-bus MG is provided in Fig. 7 and the dependency of the delay margin on the parameters of the proposed method is shown in Fig. 8.

TABLE 1. Power stage parameters of the tested multi-MG.

Symbol	Description	Value
V_{DC}	DC voltage	800 V
V_n	RMS AC rated voltage	400 V
P_{rated}	Rated active power of DGs	15 kW
Q_{rated}	Rated reactive power of DGs	6 kVar
f_n	Nominal frequency	50 Hz
F_s	Switching frequency	15 kHz
Z_{12}	Line impedances	0.1184 Ω + 0.377 mH
Z_{23}		0.3156 Ω + 1.005 mH
Z_{34}		0.2367 Ω + 0.754 mH
Z_{45}		0.1578 Ω + 0.503 mH
Z_{56}		0.0789 Ω + 0.251 mH
Z_{67}		0.1184 Ω + 0.377 mH
Z_{78}		0.2763 Ω + 0.879 mH
Z_{89}		0.1184 Ω + 0.377 mH
L_1	Load powers at nominal values	5 kW + 0.5 kVar
L_2		8 kW + 1.5 kVar
L_3		5 kW + 1 kVar
L_4		4 kW + 1 kVar
L_5		5 kW + 2 kVar
L_6		5 kW + 2 kVar
L_7		4 kW + 0.5 kVar
L_8		5 kW
L_9		20 kW + 5 kVar

1) IMPACT OF CONTROLLER PARAMETERS ON STABILITY MARGIN

Fig. 7 only shows the dominant eigenvalues that has a significant impact on system stability when varying the secondary controller parameters $K_{\Delta V}$ and $K_{\Delta\omega}$. Initial values 0.005 and 0.03 of $K_{\Delta\omega}$ and $K_{\Delta V}$ have been chosen as yielding

TABLE 2. Controller parameters.

Type	Symbol	Description	Value
AHO-based primary control	V_{DC}	Capacitance	0.2495 F
	V_n	Inductance	40.627 µH
	ξ	Speed constant	16.1107 1/sV2
	X_n	Nominal oscillation amplitude	1 V
CDP-based secondary control	K_P	Secondary gains	0.03
	K_Q		0.005

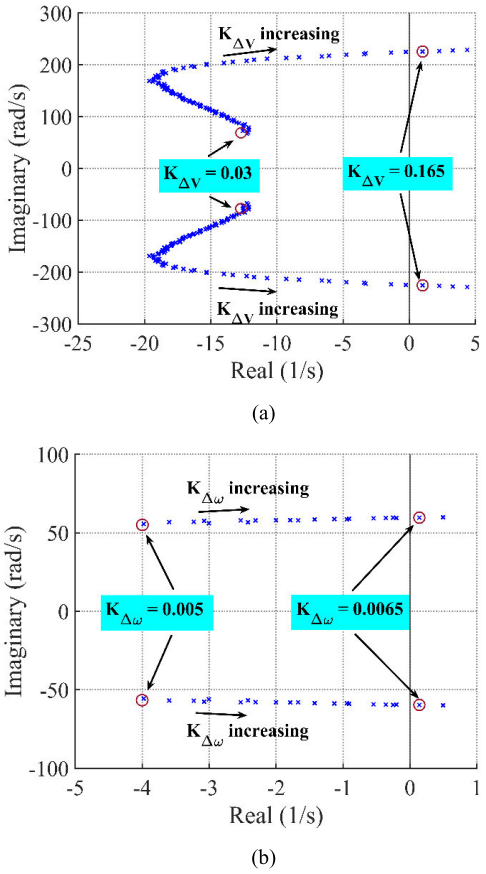

FIGURE 7. Root loci of the dominant eigenvalues of the tested system considering the changes of the CDP parameters: (a) $K_{\Delta V}$ is varied while $K_{\Delta\omega}$ is constant, (b) $K_{\Delta\omega}$ is varied while $K_{\Delta V}$ is constant.

feasible operation and reasonably good performance. Further tuning of these values is possible based on the analysis below. The results show that:

When $K_{\Delta\omega} = 0.005$, and $K_{\Delta V}$ increases from 0.03 to 0.171 (see Fig. 7a), the stability margin of the system increases at first (the dominant eigenvalues move to the far left of the stable region) and then decreases (the dominant eigenvalues move to the unstable region). The dominant eigenvalues cross the zero axis at $K_{\Delta V} = 0.165$ indicated that the system becomes unstable when $K_{\Delta V} \geq 0.165$.

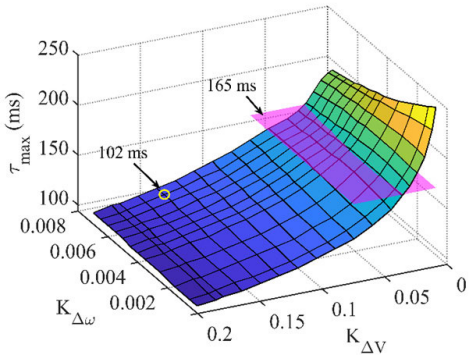

FIGURE 8. Delay margin as a function of CDP parameters.

When $K_{\Delta V} = 0.03$, the stability margin quickly reduces when $K_{\Delta\omega}$ increases from 0.005 to just 0.007 (see Fig. 7b). The system becomes unstable when $K_{\Delta\omega} \geq 0.0065$. The above analysis shows that the control parameter $K_{\Delta\omega}$ has more impact on the system stability than $K_{\Delta V}$. It is consistent with the basic theory of the VOC as $K_{\Delta\omega}$ influents the frequency of the VOC, thus the synchronization characteristic of VOC is affected.

2) IMPACT OF CONTROLLER PARAMETERS ON DELAY MARGIN

In this case study, we use the concept of delay margin (τ_{max}) [16] to evaluate the impact of the communication time delay on system stability. Delay margin is the maximum delay, for which the system is stable. Higher delay margin might be desired in case of lower quality communication infrastructure that presents higher communication latency. Fig. 8 shows the change of the delay margin when both secondary control parameters $K_{\Delta V}$ and $K_{\Delta\omega}$ vary around values from the previous section, that is, around 0.03 and 0.005, respectively. The delay margin corresponding to a given pair of secondary control power-sharing parameters is determined by deriving eigenvalues of delayed system and observing for what delay the eigenvalues related to communication time delay enter the right half-plane.

Fig. 8 indicates that both $K_{\Delta V}$ and $K_{\Delta\omega}$ have some impacts on the delay margin. The value of $K_{\Delta V}$ affects more significantly and lower $K_{\Delta V}$ increases the delay margin. Similarly, lower $K_{\Delta\omega}$ increases delay margin, but only in the region of lower $K_{\Delta V}$ values, while the impact is minor for higher $K_{\Delta V}$. The highest delay margin (165 ms) in the analyzed region can be obtained for smaller values of both $K_{\Delta V}$ and $K_{\Delta\omega}$ and the lowest delay margin (94 ms) for higher $K_{\Delta V}$, but also for lowest $K_{\Delta\omega}$. It should be noted that for some values of these parameters, which provide a higher delay margin, the dynamic response of the secondary control might be slower, what on the other hand, might be undesired depending on the design. Therefore, in general, both margin delay and dynamic response of the system have to be considered in the design process. Additionally, delay margin can be increased

with additional delay compensation methods in the primary and secondary controllers.

V. SIMULATION RESULTS AND DISCUSSION

In this section, we validate the performance of the proposed CDP for both power-sharing and synchronization in terms of steady-state error and dynamic performance, by using time-domain simulations in the real-time Opal-RT platform. The tested 9-bus MG shown in Fig. 3 consists of 5 AHO-based DGs and 9 loads. The feeders are represented by different serial RL branches. The blue-dotted lines represent communication link among DGs and between leading DG(s) and SC. Fig. 9 presents a photo of the experimental setup implemented at the laboratory of the institute for Automation of Complex Power System (ACS) – RWTH Aachen University. The parameters of the power stage and proposed controller are presented in Table 1 and 2, respectively. The choice of these parameters for VOC-based DGs is based on [17] and explained there in more detail.

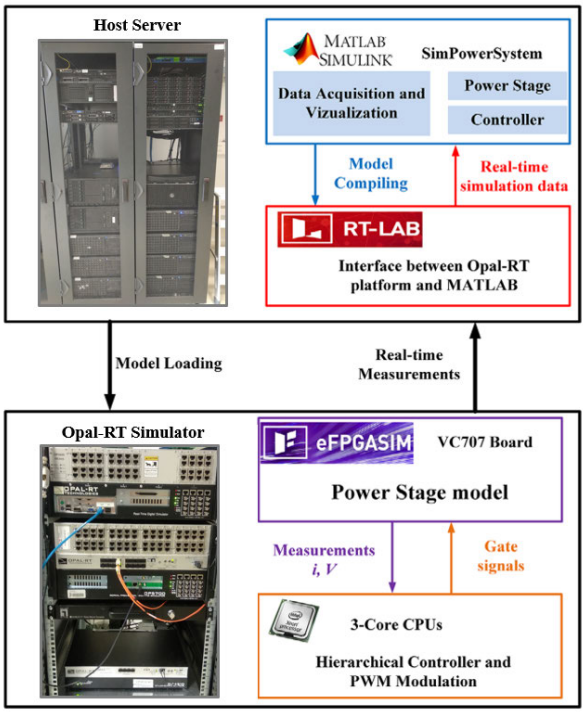

FIGURE 9. Experimental setup of the tested system.

The value of the coefficients of the proposed synchronization control are $K_{|\Delta V|} = 200$, and $K_{|f-\theta|} = 4000$, respectively. The grid is modeled as an ideal three-phase voltage source connected in series with an impedance $Z_N = 0.1 + j0.1\Omega$. In the beginning, the MG operates under islanded mode without the proposed secondary controller. CDP then is activated at time t = 2 s to improve power-sharing accuracy among DGs. At time t = 8 s, the request to connect to the main grid is sent from the upper control level, resulting in the activation of the proposed synchronization approach. The MG is connected to the main grid at time t = 16 s.

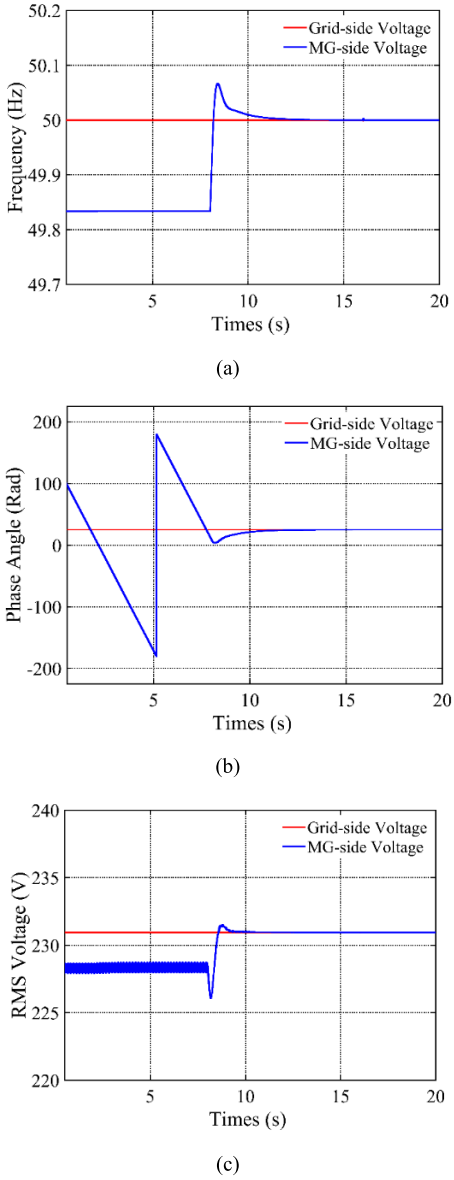

FIGURE 10. Voltage at two sides of the SS in Case 1: a) frequency, b) phase angle, and c) magnitude.

Three different case studies were analyzed in the subsequent sections, namely centralized synchronization, distributed synchronization, and influence of communication time-delay.

A. CASE 1: CENTRALIZED SYNCHRONIZATION

In this case study, the objective is to validate the performance of the proposed synchronization strategy under an all-to-all communication network for synchronization, i.e., the synchronization signals are sent from the SC to every DG in MG simultaneously without communication time delay. Initially, MG operates in islanded mode, with the frequency and voltage at bus B stabilizes at 49.85 Hz and 0.99 pu, respectively. Meanwhile, the utility grid frequency and phase angle are constant 50 Hz and 25 degree, and the voltage measured at bus

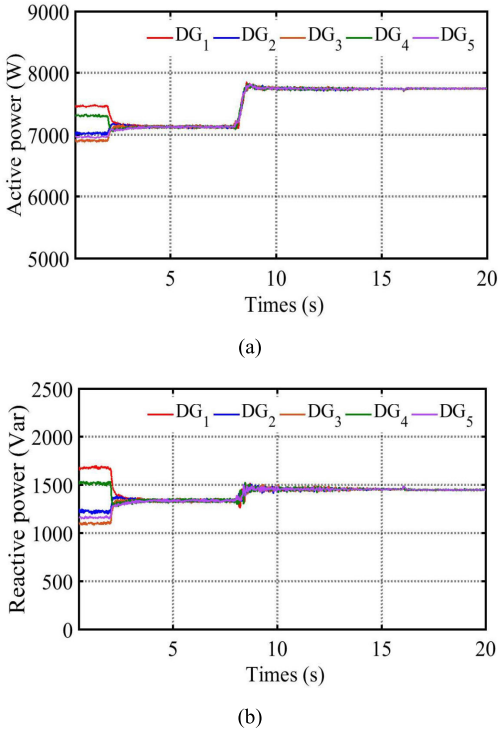

FIGURE 11. Variation of DG power outputs in Case 1: a) Active power, b) Reactive power.

A is 1.0 pu. The proposed CDP and synchronization control are activated at t = 2 s and t = 8 s, respectively. The simulation results are shown in Fig. 10 and Fig. 11.

Fig. 10 shows the frequency, phase angle, and magnitude of the voltage at bus A and B, respectively. When the proposed synchronization control is activated, the voltage frequency and magnitude at the bus B quickly tracks the utility grid voltage in around 2.5 seconds with a negligible transient. The phase angle difference between MG side voltage and main grid voltage when the proposed control is activated (t = 8 s) is 24 degree. After 1.6 seconds after the proposed control is enabled, the phase angle difference drops well below 1 degree. Fig. 11 presents the variation of the DG power outputs under the activation of the proposed CDP and synchronization control. As Fig.11 shows, before t = 8 s, all DGs share the load power equally as an effect of the proposed CDP. When the proposed synchronization control is activated, both active and reactive power output of DGs simultaneously converges to new equilibrium points so that the voltage at bus B synchronizes with that of bus A.

As the proposed synchronization controller sends the same additional control signals to the input of all CDP, the DG power outputs show identical transient behavior. At t = 16 s, MG is smoothly connected to the utility grid. Small transients in a short time of the power outputs of all DGs indicate that the inrush current flowing through the SS is significantly small during the connection process.

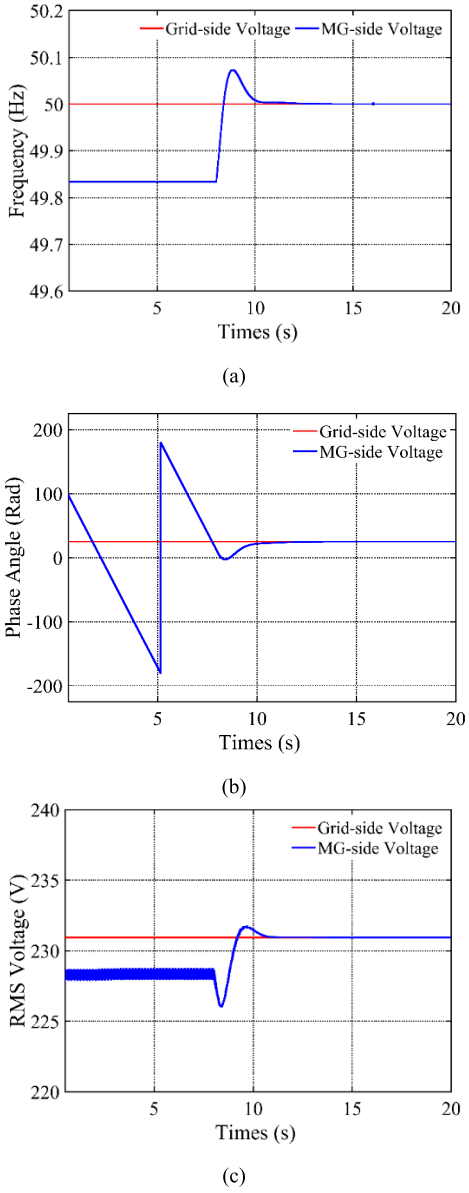

FIGURE 12. Voltage at two sides of the SS in Case 2: a) frequency, b) phase angle, and c) magnitude.

B. CASE 2: DISTRIBUTED SYNCHRONIZATION

In this case study, the synchronization signals are assumed to be received only by the CDP of the DG_3. The initial conditions of the MG are the same as case 1. The objective of this case study is to validate the performance of the proposed synchronization control under a fully distributed manner where DG_3 is the only leading DG, communicating with SC. Whereas the communications of other DGs keep unchanged. Simulation results of the voltage and power variations are presented in Fig. 12 and Fig. 13, respectively.

As Fig. 12 shows, when the proposed synchronization control is enabled at t = 8 s, the voltage at bus B closely track the voltage at bus A with slightly longer transient, in comparison to case 1. Simulation results also show a small overshoot

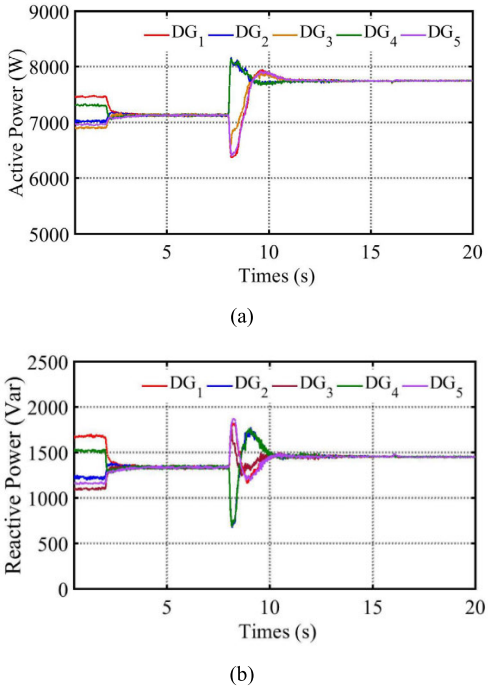

FIGURE 13. Variation of DG power outputs in Case 2: a) Active power, b) Reactive power.

in case of frequency, and negligible undershoot in case of phase angle. However, these transients vanish quickly, and after 1.8 seconds, the phase angle difference drops well below 1 degree. The simulation results in Fig. 13 show that the highest overshoot is observed in both active and reactive power output of DG_3 since the control law of the CDP corresponding to DG_3 is influenced directly by the proposed synchronization control, while the other DGs receive the setpoints already averaged by at least CDP of the leading DG. The transient effects of the proposed CDP vanish completely in around 3 seconds after the control is enabled, and at the same time, the power outputs of all DGs converge to a new equilibrium point to share the load equally. The synchronization requirements from IEEE Standard 1547.2-2008 and from [10] are then fully satisfied, and MG can be smoothly connected to the main grid.

The above analysis shows that there is a trade-off between technical and economic perspectives when using the proposed secondary control approach. Better dynamic performance is achieved with the high density of the communication network, which might generate higher investment costs and exposition to problems with communication failure, security or compatibility. The proposed distributed approach provides a slower dynamic response, but equally accurate steady-state performance with a minimum number of required communication links. It might make the proposed approach more practical in systems where distributed communication or a certain degree of it is necessary.

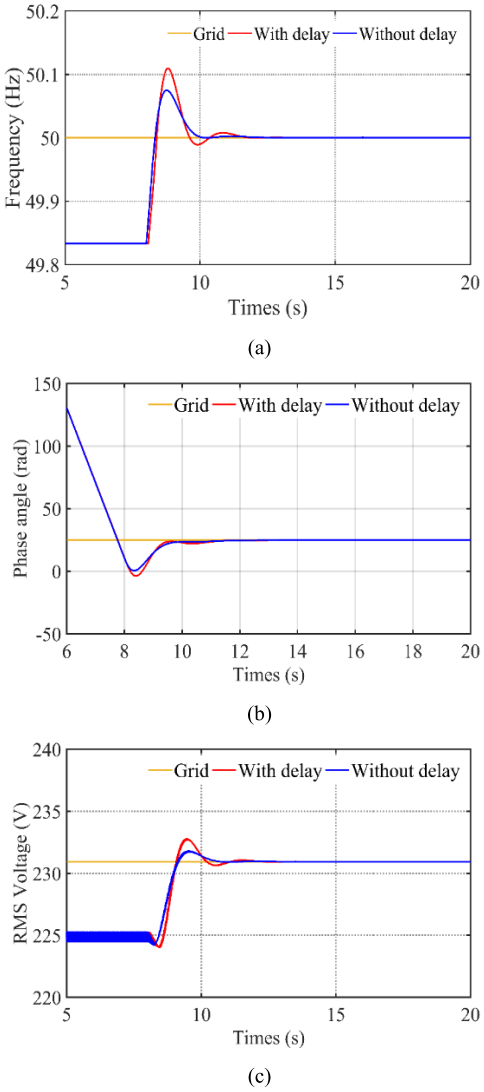

FIGURE 14. Voltage at two sides of the SS in Case 3: a) frequency, b) phase angle, and c) magnitude.

TABLE 3. Time delay of communication links.

Communication link	Time-delay (ms)
$DG_1 \leftrightarrow DG_2$	100
$DG_2 \leftrightarrow DG_3$	70
$DG_3 \leftrightarrow DG_4$	80
$DG_4 \leftrightarrow DG_5$	90
$SC \leftrightarrow DG_3$	70

C. CASE 3: INFLUENCE OF COMMUNICATION TIME-DELAY

This case study aims at demonstrating the performance of the proposed synchronization control strategy under the occurrence of the communication time-delay between DGs and between leading DG(s) and SC.

In this scenario, the time-delays of communication links are presented in Table 3. These delays are assumed realistic in

a good quality communication infrastructure, but not a low-latency infrastructure dedicated for DG-to-DG communication. The rest of the simulation conditions are the same as those in Case 2. Simulation results are presented in Fig. 14. The simulation results show that even with a large time delay, the dynamic response of the proposed CDP is reduced by less than 1% (in terms of overshoot and settling time), compared to the case without communication time-delays. The MG voltage is still successfully synchronized with the utility grid in around 6 seconds, and the MG can seamlessly connect to the main grid from time t = 12 s. Therefore, the proposed method is robust under considerable communication time delay.

VI. CONCLUSION

This paper proposes a hierarchical control strategy for power-sharing and for a smooth transition of multi-bus MGs from islanded mode to grid-connected. The strategy includes an AHO-based primary control layer jointly with secondary control layer, which adopts an average consensus distributed protocol towards achieving proportional power-sharing among DGs and simultaneously synchronization to the external grid. Specifically, the proposed control strategy aims to reduce inaccuracy in power-sharing in normal operation and furthermore synchronizes voltage at both sides of the static switch in synchronization mode that allows the MG to seamlessly connect to the main grid without direct frequency and phase angle measurements. The eigenvalue-based small-signal stability analysis is performed to analyze the dependency of the controller parameters and communication time-delay on the system dynamics.

The results in real-time simulation in the Opal-RT platform show that:

1) In normal islanded operation, the proposed control strategy can effectively eliminate the power-sharing errors among DGs caused by the different line impedances and load locations. The active power-sharing inaccuracy is nullified, while there is a minor steady-state error of 0.7% in reactive power-sharing.
2) The proposed distributed control strategy enables the MG-side voltage to synchronize with the grid-side voltage in synchronization mode. The magnitude and frequency difference between the voltage at two sides of SS are eliminated in about 3 seconds. Meanwhile, the phase angle difference is dropped from 24 degree to less than 1 degree with the effect of the proposed method, thus allowing MG to seamlessly connect to the main grid.
3) The performance of the proposed distributed control strategy is slightly less than the centralized control method, in terms of settling time. However, this performance reduction (e.g., the settling time in a centralized case is 2.5 seconds, while in the proposed method is 3 seconds) may be counterbalanced by the technical and economic advantages of the distributed solution.

The eigenvalue-based stability analysis presents the approach to controller parameters fitting in order to accomplish prospective requirements of system dynamics and communication infrastructure. The results of the analysis can be used to verify the system stability with a certain set of controller parameters and communication time delays, and to optimize controller parameters and delay margin that keeps the system stable. In addition, the small-signal model is developed independently on the number and location of DGs, loads, and branches. Thus, it can be used in various structures of radial multi-bus MGs.

An important direction for future research is to improve the proposed control strategy under unbalanced load conditions, as such loads are common in low-voltage MGs. Furthermore, the stability analysis should be extended to transient stability analysis in order to include large deviations like synchronization actions or significant imbalances. The implementation of Power Hardware-in-the-Loop (PHiL) in laboratory environment additionally to the provided CHiL is also an essential step to prove the practical application of the proposed method.

REFERENCES

[1] P. Piagi and R. H. Lasseter, "Autonomous control of microgrids," in *Proc. IEEE Power Eng. Soc. Gen. Meeting*, Jun. 2006, p. 8, doi: 10.1109/PES.2006.1708993.

[2] D. Shi, X. Chen, Z. Wang, X. Zhang, Z. Yu, X. Wang, and D. Bian, "A distributed cooperative control framework for synchronized reconnection of a multi-bus microgrid," *IEEE Trans. Smart Grid*, vol. 9, no. 6, pp. 6646–6655, Nov. 2018, doi: 10.1109/TSG.2017.2717806.

[3] C. Dou, Z. Zhang, D. Yue, and M. Song, "Improved droop control based on virtual impedance and virtual power source in low-voltage microgrid," *IET Gener., Transmiss. Distrib.*, vol. 11, no. 4, pp. 1046–1054, Mar. 2017, doi: 10.1049/iet-gtd.2016.1492.

[4] Z. Cheng, Z. Li, J. Liang, J. Gao, J. Si, and S. Li, "Distributed economic power dispatch and bus voltage control for droop-controlled DC microgrids," *Energies*, vol. 12, no. 7, p. 1400, Apr. 2019, doi: 10.3390/en12071400.

[5] B. B. Johnson, S. V. Dhople, A. O. Hamadeh, and P. T. Krein, "Synchronization of parallel single-phase inverters with virtual oscillator control," *IEEE Trans. Power Electron.*, vol. 29, no. 11, pp. 6124–6138, Nov. 2014, doi: 10.1109/TPEL.2013.2296292.

[6] M. Karimi-Ghartemani, "Universal integrated synchronization and control for single-phase DC/AC converters," *IEEE Trans. Power Electron.*, vol. 30, no. 3, pp. 1544–1557, Mar. 2015, doi: 10.1109/TPEL.2014.2304459.

[7] G. M. S. Azevedo, F. Bradaschia, M. C. Cavalcanti, F. A. S. Neves, J. Rocabert, and P. Rodriguez, "Safe transient operation of microgrids based on master-slave configuration," in *Proc. IEEE Energy Convers. Congr. Expo.*, Sep. 2011, pp. 2191–2195, doi: 10.1109/ECCE.2011.6064058.

[8] J. Chen, S. Hou, and J. Chen, "Seamless mode transfer control for master–slavemicrogrid," *IET Power Electron.*, vol. 12, no. 12, pp. 3158–3165, Oct. 2019, doi: 10.1049/iet-pel.2018.6286.

[9] C. Cho, J.-H. Jeon, J.-Y. Kim, S. Kwon, K. Park, and S. Kim, "Active synchronizing control of a microgrid," *IEEE Trans. Power Electron.*, vol. 26, no. 12, pp. 3707–3719, Dec. 2011, doi: 10.1109/TPEL.2011.2162532.

[10] F. Tang, J. M. Guerrero, J. C. Vasquez, D. Wu, and L. Meng, "Distributed active synchronization strategy for microgrid seamless reconnection to the grid under unbalance and harmonic distortion," *IEEE Trans. Smart Grid*, vol. 6, no. 6, pp. 2757–2769, Nov. 2015, doi: 10.1109/TSG.2015.2406668.

[11] D. Gros, M. Colombino, J.-S. Brouillon, and F. Dorfler, "The effect of transmission-line dynamics on grid-forming dispatchable virtual oscillator control," *IEEE Trans. Control Netw. Syst.*, vol. 6, no. 3, pp. 1148–1160, Sep. 2019, doi: 10.1109/TCNS.2019.2921347.

[12] Z. Li, Z. Cheng, J. Liang, J. Si, L. Dong, and S. Li, "Distributed event-triggered secondary control for economic dispatch and frequency restoration control of droop-controlled AC microgrids," *IEEE Trans. Sustain. Energy*, vol. 11, no. 3, pp. 1938–1950, Jul. 2020, doi: 10.1109/TSTE.2019.2946740.

[13] Z. Zhang, Y. Mishra, D. Yue, C. Dou, B. Zhang, and Y.-C. Tian, "Delay-tolerant predictive power compensation control for photovoltaic voltage regulation," *IEEE Trans. Ind. Informat.*, vol. 17, no. 7, pp. 4545–4554, Jul. 2021, doi: 10.1109/TII.2020.3024069.

[14] M. Lu, S. Dutta, V. Purba, S. Dhople, and B. Johnson, "A grid-compatible virtual oscillator controller: Analysis and design," in *Proc. IEEE Energy Convers. Congr. Expo. (ECCE)*, Sep. 2019, pp. 2643–2649, doi: 10.1109/ECCE.2019.8913128.

[15] T. T. Tran, I. Sowa, D. Raisz, and A. Monti, "An average consensus-based power-sharing among VOC-based distributed generations in multi-bus islanded microgrids," *IET Gener., Transmiss. Distrib.*, vol. 15, no. 4, pp. 792–807, Feb. 2021, doi: 10.1049/gtd2.12059.

[16] X. Wu, Y. Xu, J. He, C. Shen, G. Chen, J. C. Vasquez, and J. M. Guerrero, "Delay-dependent small-signal stability analysis and compensation method for distributed secondary control of microgrids," *IEEE Access*, vol. 7, pp. 170919–170935, 2019, doi: 10.1109/ACCESS.2019.2955090.

[17] T. Heins, T. Tran, D. Raisz, and A. Monti, "Power control of Andronov-Hopf oscillator based distributed generation in grid-connected microgrids," in *Advances in Engineering Research and Application*, K.-U. Sattler, D. C. Nguyen, N. P. Vu, B. T. Long, and H. Puta, Eds. Cham, Switzerland: Springer, 2021, pp. 675–687.

IGOR SOWA received the M.Sc. degree in electrical engineering from KTH University, Stockholm, Sweden, and UPC University, Barcelona, Spain, in 2016. He is currently pursuing the Ph.D. degree with the Institute for Complex Power Systems, RWTH University, Aachen, Germany. Since 2016, he has been a Research Associate with the Institute for Complex Power Systems, RWTH University. His research interests include power system dynamics and control, as well as communication and monitoring in modern power systems and microgrids.

TRUNG THAI TRAN received the M.Sc. degree in electrical engineering from Chonnam National University, Gwangju, South Korea, in 2012, and the Ph.D. degree in electrical engineering from the E. ON Energy Research Center, Institute for Automation of Complex Power Systems, RWTH Aachen University, Aachen, Germany, in 2020. Since 2010, he has been working as a Lecturer with the Thai Nguyen University of Technology, Vietnam. His research interests include power system operation and control, control strategies applied to distributed energy resources in microgrids, and real-time simulation.

TOBIAS HEINS received the M.Sc. degree in electrical engineering from RWTH Aachen University, in 2020. He is currently a Research Associate with the E. ON Energy Research Center, Institute for Automation of Complex Power Systems, RWTH Aachen University. His research interests include control strategies for distributed energy resources and power systems.

DAVID RAISZ (Senior Member, IEEE) received the M.Sc. and Ph.D. degrees in electrical engineering from the Budapest University of Technology and Economics (BUTE), Budapest, Hungary, in 2000 and 2011 respectively. From 1999 to 2001, he was a Guest Researcher with the Graz University of Technology, Austria. From 2012 to 2016, he led the Power Systems and Environment Group, Department of Electric Power Engineering, BUTE, as an Associate Professor. In 2017, he joined the E. ON Energy Research Center, Institute for Automation of Complex Power System, RWTH Aachen University. He has been working on or leading more than 40 industrial and research projects.

ANTONELLO MONTI (Senior Member, IEEE) received the M.Sc. *(summa cum laude)* and Ph.D. degrees in electrical engineering from Politecnico di Milano, Italy, in 1989 and 1994, respectively. He started his career in Ansaldo Industria and then moved in 1995 to Politecnico di Milano as an Assistant Professor. In 2000, he joined the Department of Electrical Engineering, University of South Carolina, USA, as an Associate Professor and then a Full Professor. Since 2008, he has been the Director of the E. ON Energy Research Center, Institute for Automation of Complex Power System, RWTH Aachen University. He is the author or a coauthor of more than 300 peer-reviewed articles published in international journals and in the proceedings of international conferences. He was a recipient of the 2017 IEEE Innovation in Societal Infrastructure Award. He is an Associate Editor of the IEEE Systems Journal and *IEEE Electrification Magazine*, a member of the Editorial Board of *SEGAN* journal (Elsevier), and a member of the founding board of the *Energy Informatics* journal (Springer).